Microplate-compatible total internal reflection fluorescence microscopy for receptor pharmacology

Minghan Chen,[1,a)] Natalya V. Zaytseva,[1,a)] Qi Wu,[1] Min Li,[2] and Ye Fang[1,b)]
[1]*Biochemical Technologies, Science and Technology Division, Corning Incorporated, Corning, New York 14831, USA*
[2]*The Solomon H. Snyder Department of Neuroscience and High Throughput Biology Center, Johns Hopkins University School of Medicine, Baltimore, Maryland 21205, USA*

(Received 18 March 2013; accepted 24 April 2013; published online 14 May 2013)

We report the use of total internal reflection fluorescence (TIRF) microscopy for analyzing receptor pharmacology and the development of a microplate-compatible TIRF imaging system. Using stably expressed green fluorescence protein tagged β_2-adrenergic receptor as the reporter, we found that the activation of different receptors results in distinct kinetic signatures of the TIRF intensity of cells. These TIRF signatures closely resemble the characteristics of their respective label-free dynamic mass redistribution signals in the same cells. This suggests that TIRF in microplate can be used for profiling and screening drugs. © *2013 AIP Publishing LLC*.
[http://dx.doi.org/10.1063/1.4805041]

Total internal reflection fluorescence (TIRF) microscopy has been used as a single molecule/organelle tracking technique[1] to study various fundamental aspects of cell biology, including cell adhesion,[2] receptor organization and trafficking,[3,4] exocytosis,[5] and micro-morphological structures and dynamics.[6] TIRF microscopy employs a surface bound evanescent wave to excite fluorophores very near a solid surface, given that the light undergoing total internal reflection creates the evanescent wave penetrating and exponentially decaying into the aqueous solution. However, current TIRF microscopy is single well based and has little use in high content/throughput screening and for characterizing receptor pharmacology, due to the inherent complexity of current instrumental setup and experimental procedures.[7,8] Furthermore, in the recent years, amassing data has shown that label-free evanescent wave-based resonant waveguide grating (RWG) biosensor reproduces the functional consequence of a drug-receptor interaction in cells into a dynamic mass redistribution (DMR) signature,[9,10] permitting cell phenotypic profiling and screening of drug-receptor interactions with high throughput.[11–13] Herein, we hypothesize and confirm that TIRF microscopy can be used to characterize receptor pharmacology in a way complementary to these label-free evanescent wave biosensors. We also report the development of a microplate-compatible TIRF imaging system to speed up TIRF measurements.

We first compared the label-free DMR signals arising from the activation of several receptors with their respective TIRF signals. Both types of signals were obtained in an engineered human embryonic kidney-293 (HEK293) cell line which stably expresses β_2-adrenergic receptor (β_2AR) with green fluorescent protein (GFP) tag at its C-terminal (β_2AR-GFP). The β_2AR-GFP was used as a cell surface fluorescence reporter for TIRF measurements. The stable cell line was prepared by transfecting HEK293 cells with human pCMV-β_2AR-GFP plasmid (OriGene Technologies, Inc., Rockville, MD, USA) using Lipofectamine™ LTX and Plus Reagent (Invitrogen, Grand Island, NY, USA) in a 6-well cell culture plate, followed by selection using 500 μg/ml G418 Geneticin® (Invitrogen) the next day, and then clone picking based on the GFP signal and pattern.

The DMR signals were obtained under ambient condition (~23 °C) using Epic® BT system, a recently developed whole microplate-based RWG biosensor imager (Corning Inc., Corning, NY, USA).[14] The HEK-β_2AR-GFP cells were seeded at a density of 12 000 cells per well and cultured onto Epic® fibronectin coated 384-well biosensor microplates (Corning). After overnight culture in the complete medium (that is, minimum essential medium (MEM) with GlutaMax™ supplemented with 10% fatal bovine serum and antibiotics) at 37 °C/5% CO_2, the confluent cells were then washed and maintained in the assay vehicle (HBSS; 1 × Hank's balanced salt solution, 20 mM Hepes-KOH, pH 7.1) for about 1 h before stimulation. Results showed that the treatment with the assay vehicle led to little DMR (Fig. 1(a)), while the treatment with several ligands all triggered robust DMR signals but with distinct kinetics and amplitudes (Figs. 1(b)–1(f)). Both epinephrine and isoproterenol are two agonists for the β_2AR,[15] while epidermal growth factor (EGF) is an agonist for EGF receptor,[10,16] Adenosine-5′-triphosphate (ATP) an agonist for P2Y purinergic receptors,[17] L-Seryl-L-phenylalanyl-L-leucyl-L-leucyl-L-Arginine amide (SFLLR) a peptidic agonist for protease activated receptor-1,[18] and TBB (4,5,6,7-tetrabromobenzotriazole) a multi-kinase inhibitor.[12,19] These results confirm that DMR assays are capable of multi-target profiling.

The TIRF measurements were carried out under ambient condition using conventional TIRF microscopy equipped with a low-noise, light-sensitive Andor iXon+ electron multiplying charge-coupled device (EM-CCD) camera (Nikon Instruments, Inc., Melville, NY, USA). The HEK-β_2AR-GFP cells were seeded at a density of 150 000 cells per well into fibronectin coated 13-mm glass bottom wells of 24-well Mattek plates (MatTek Co., Ashland, MA, USA). After overnight culture, the confluent cells were washed and maintained in the assay vehicle. Time-elapsed TIRF images with an interval

[a)]M. Chen and N. V. Zaytseva contributed equally to this work.
[b)]Electronic mail: fangy2@corning.com; Tel: +607-9747203.

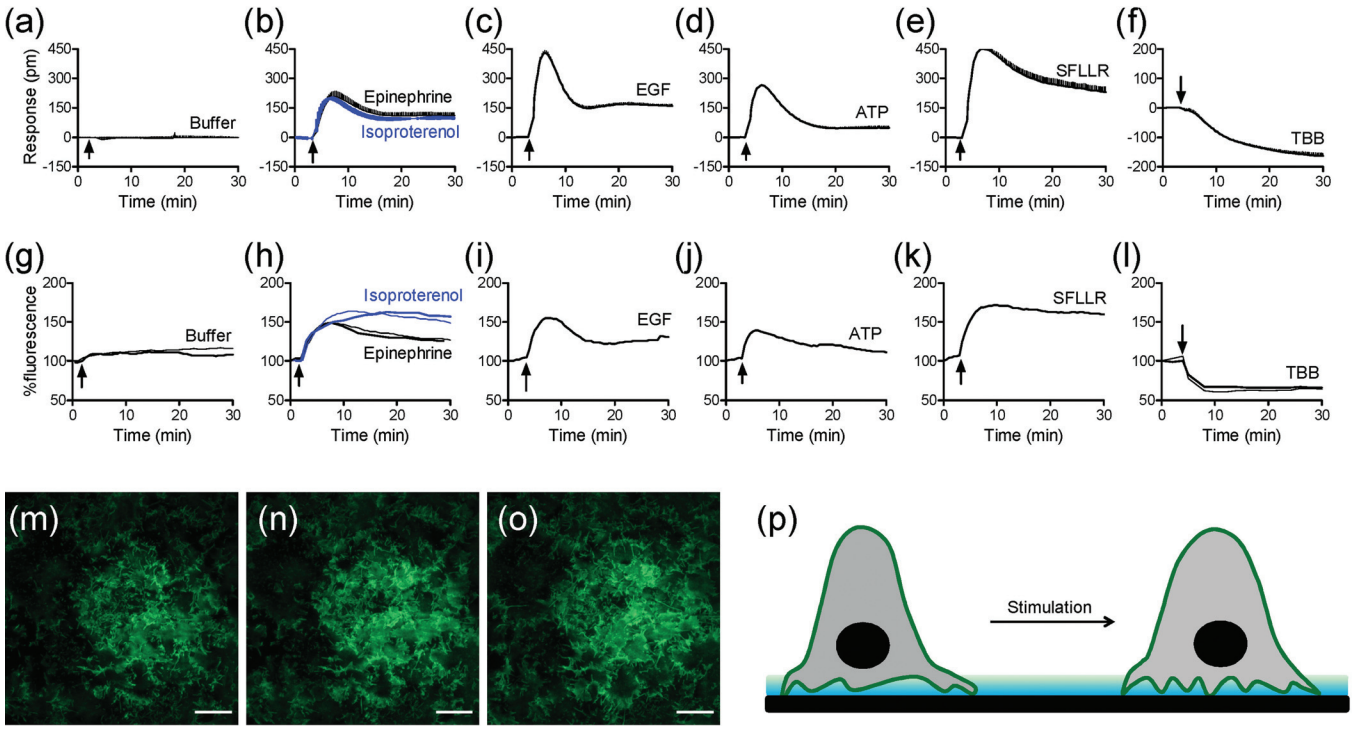

FIG. 1. Characteristics of DMR and TIRF signals arising from the receptor activation in HEK-β_2AR-GFP cells. (a-f) Real-time DMR signals induced by: the assay vehicle (a), 10 μM epinephrine and 10 μM isoproterenol (b), 32 nM EGF (c), 10 μM ATP (d), 10 μM SFLLR (e), and 10 μM TBB (f). (g-l) Real-time TIRF signals induced by: the assay vehicle (g), 10 μM epinephrine and 10 μM isoproterenol (h), 32 nM EGF (i), 10 μM ATP (j), 10 μM SFLLR (k), and 10 μM TBB (l). (m-o) False-colored TIRF images before (m), and 2 min (n) and 10 min (o) after the stimulation with 10 μM epinephrine. (p) Schematic drawing showing the mechanism for the epinephrine induced increase in TIRF signal. The data in (a-f) show mean$\pm$s.d. of 8 replicates. Scale bar in m-o is 10μm.

of 30 s or 1 min were obtained using a 488 nm argon laser of 1mW power, coupled with a 100×, 1.49 numerical aperture TIRF objective (Nikon) using immersion oil with n = 1.515 at 23 °C. Each sample was monitored for at least 5 min to achieve a steady TIRF baseline before compound addition. The fluorescence intensity at 5 min was normalized to 100%. Results showed that the treatment with the assay vehicle led to little change in TIRF intensity (Fig. 1(g)). In contrast, the treatments with the same set of ligands all resulted in clear changes in TIRF but with different characteristics in kinetics and amplitude (Figs. 1(h)–1(l)). Strikingly interesting is that the signature of every ligand-induced TIRF kinetic profile obtained closely resembles its corresponding DMR signal. Such a similarity is originated from the fact that both label-free DMR and TIRF measurements are based on a surface bound evanescent wave. Also true is that there are clear differences in fine characteristics between the DMR and TIRF signals of every ligand. This is probably due to the difference in measurement between the two techniques. RWG biosensor is mostly sensitive to dynamic redistribution of cellular matters within the sensing volume (~150 nm), leading to a DMR which is an integrated response.[11] In contrast, TIRF is a direct function of the distances of fluorescent receptors at the cell surface but within 100 nm near the glass surface.[6] Given the short penetration depth of the evanescent wave, only the fluorescent receptors located at the cell surface membrane near the substrate surface contribute to the TIRF signal. This was evidenced by the time lapsed TIRF images of the cells before and after treatment with epinephrine (Figs. 1(m)–1(o)). The increasing TIRF observed after epinephrine stimulation suggests that the basal cell membrane becomes closer to the surface (Fig. 1(p)). Collectively, these results suggest that the TIRF measurements can provide useful information for assessing receptor pharmacology in a way that is complementary to the label-free DMR results.

Next, we developed a prism-based and microplate-compatible TIRF imaging system to speed up TIRF measurements. A 488 nm diode laser (Continuous Wave 488 nm Solid-State Laser, JDSU, Milpitas, CA, USA) is used to launch a light beam into glass substrate with the aid of a right-angle prism (5 mm BBAR Coated Right Angle Prism, VIS 0° Coated, Edmund Optics Inc., Barrington, NJ, USA) (Fig. 2(a)). Immersion oil is applied to fill the gap between the prism and the plate substrate. When the laser incident angle exceeds a critical angle, total internal reflection is observed and the evanescent wave generated at the boundary of glass substrate and aqueous solution is then used to excite cell surface β_2-AR-GFPs within the sensing sampling depth. Instead of expensive EM-CCD, a regular cooled CCD camera (Nikon DS-Qil, Nikon), together with a Nikon CF plan SLWD 50 × (0.45 NA, 13.8 mm working distance) objective and a tube lens with a 200 mm effective focal length, are used to record the TIRF images. This system can perform both epi-fluorescence and TIRF imaging, depending on the laser incident angle (Fig. 2(b)).

We fabricated 96-well glass bottom microplates by attaching a glass sheet to the bottom of a 96-well black wall hole plate using pressure sensitive adhesives. The glass with a thickness of 500 μm was first coated with stripes of aluminum thin film using sputtering method with the help of an aluminum mask. The side of the glass substrate having aluminum stripes faced outside, and the aluminum stripes were

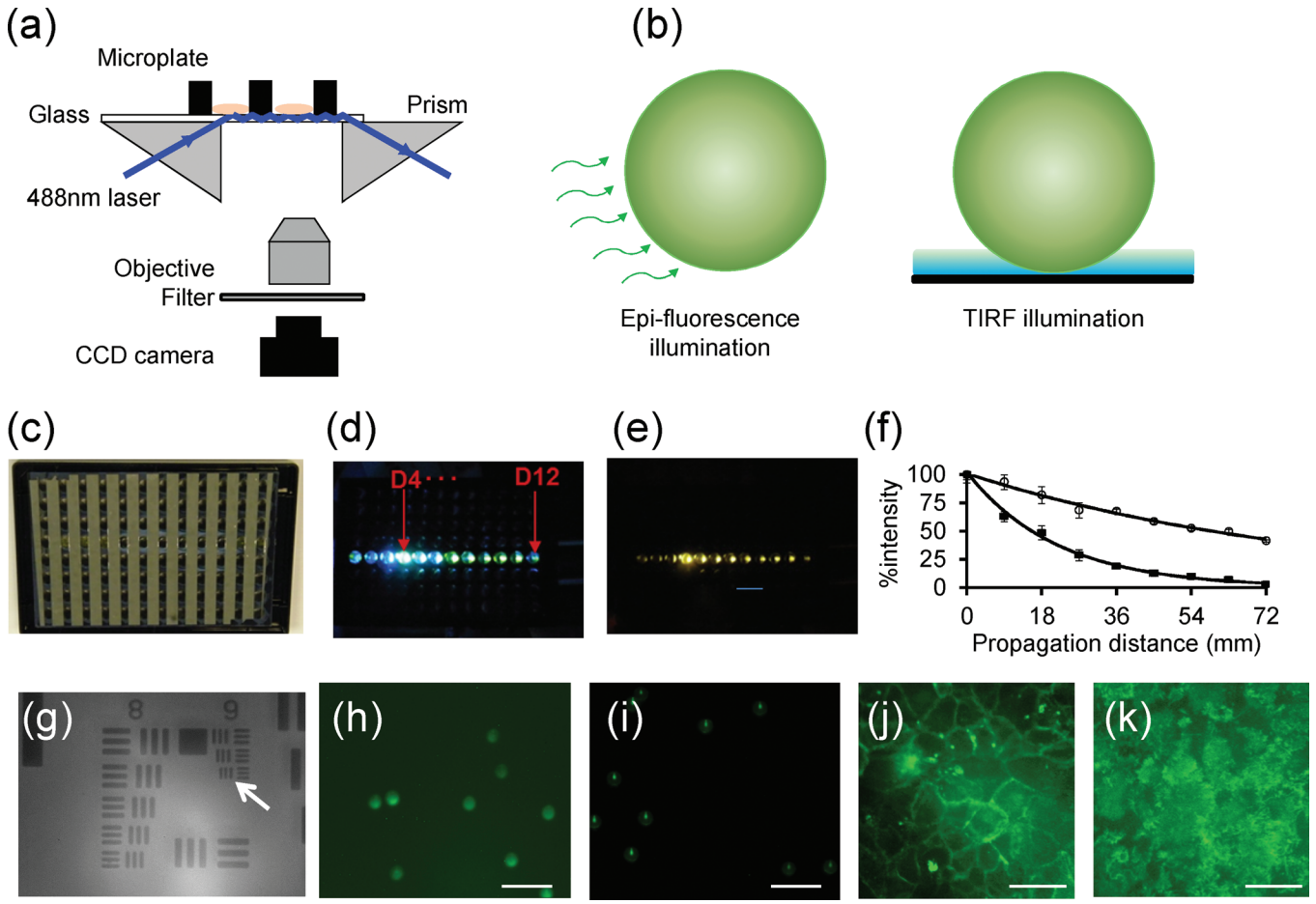

FIG. 2. Microplate-compatible TIRF imaging system. (a) Schematic drawing showing the instrument setup. A 488 nm laser light is used to illuminate the glass substrate with the aid of a right angle prism. The evanescent wave excited fluorescence is collected using an objective lens, passed through a filter and focused via a tube lens onto a CCD camera. (b) Two illumination schemes: epi-fluorescence and TIRF. (c) The back image of a glass bottom microplate to show the geometry of alumina stripes. (d) The excitation light propagates within the glass substrate after it illuminates the well D4. (e) The whole plate fluorescence observed within multi-wells by placing a filter in front of CCD camera. (f) Light intensity profile as it propagates from the well D4 to D12 within the glass substrate without (black squares) and with (open circles) the alumina stripes. (g) The transmission image of USAF target using a 50 × objective. (h) The epi-fluorescence image of 10 μm green fluorescence beads. (i) The TIRF image of the beads. (j) The epi-fluorescence image of HEK-β_2AR-GFP cells. (k) The TIRF image of the cells. Scale bar in (h-k) is 40 μm.

perpendicular to the light propagation direction, once the microplate was assembled (Fig. 2(c)). This is essential to reduce the evanescent wave attenuation and to minimize the leakage of the total internal reflection light into the adhesives between the wall of the microplate and the glass substrate, so it is possible to simultaneously illuminate multiple wells along the propagation direction. To illustrate this, a prism was attached to the left side of the microplate till it partially covers the D4 well. Once the incident angle reached the critical angle, the excitation light underwent total internal reflection and propagated within the glass plates all the way to the well D12 (Fig. 2(d)). By placing a band pass filter in front of the CCD camera, the fluorescence emission from multi-wells was observed coincidentally (Fig. 2(e)). For plates having aluminium stripes, the laser attenuation coefficient was found to be reduced by ~4 times, comparing with the plates without the stripes (Fig. 2(f)). The beam intensity attenuation coefficient was 0.045 and 0.01 mm^{-1} for the control plate without the stripes and the alumina patterned plate, respectively.

The TIRF system was calibrated by measuring the transmission image of an US Air Force target (USAF). Results showed that this system has a field of view of 150 × 112 μm and can resolve the group 9 element 3 (Fig. 2(g)), suggesting that the system has a spatial resolution of 0.78 μm. The TIRF illumination was also calibrated by imaging green fluorescence dye modified polystyrene microsphere beads of 10 μm in diameter (Invitrogen). Results showed that under epi-fluorescence illumination scheme, the bulk images of beads were obtained (Fig. 2(h)). However, with localized evanescent wave illumination the beads gave rise to much smaller dot-like morphology with small tailed structure as well as a dim ring structure (Fig. 2(i)). The dot-like morphology was due to selective excitation of the fluorophores within the bottom of the beads by the substrate bound evanescent wave. The tailed scattering was originated from the focusing effects of granular beads on the evanescent optical waves.[20,21] The dim ring structure surrounding each dot was due to the epi-fluorescence background noise. This noise can be used to calculate the signal to noise ratio of TIRF images by measuring the ratio of the averaged intensity of a TIRF dot to the dim ring fluorescence image of these fluorescent beads. We found that using the alumina patterned microplate the signal to noise ratios from D4 to D12 wells all were about 8.3, when the light was launched at the well D4. This suggests that it is possible for the present TIRF system to perform TIRF measurements with moderately higher throughput, compared to conventional

TIRF microscopy. Finally, we characterized the fluorescence images of the HEK-β2AR-GFP cells. Results showed that the epi-fluorescence is mostly concentrated at the rim of the cells (Fig. 2(j)). However, the TIRF patterns were branch-like, similar to those obtained using conventional TIRF microscopy (comparing Fig. 2(k) with Fig. 1(m)).

In summary, we have shown that conventional TRIF imaging can be used to characterize receptor pharmacology, complementary to the results obtained using label-free evanescent wave-based biosensors. We have also developed a prism based and microplate compatible TIRF imaging system that allows both epi-fluorescence and TIRF measurements. Such a system holds promise in characterizing receptor signaling and pharmacology with moderate throughput and has clear applicability to those pathways involving membrane redistribution. Given the ability to control the penetration depth of the evanescent wave using different incident angles, it is expected that this system allows for probing multiple events occurring at different locations in the cells through measuring incident angle dependent fluorescence. The TIRF imaging systems described here paves the way for profiling and screening drugs based on TIRF measurements.

This work was supported partially by National Institutes of Health under Grant 5U54MH084691 (M.L., Y.F.).

[1]Y. Sako, S. Minoguchi, and T. Yanagida, Nat. Cell Biol. **2**, 168 (2000).
[2]M. E. Berginski, E. A. Vitriol, K. M. Hahn, and S. M. Gomez, PLoS ONE **6**, e22025 (2011).
[3]J. A. Hern, A. H. Baig, G. I. Mashanov, B. Birdsall, J. E. T. Corrie, S. Lazareno, J. E. Molloy, and N. J. M. Birdsall, Proc. Natl. Acad. Sci. U.S.A. **107**, 2693 (2010).
[4]D. Calebiro, F. Rieken, J. Wagner, T. Sungkaworn, U. Zabel, A. Borzi, E. Cocucci, A. Zurn, and M. J. Lohse, Proc. Natl. Acad. Sci. U.S.A. **110**, 743 (2013).
[5]J. A. Steyer and W. Almers, Nat. Rev. Mol. Cell Biol. **2**, 268 (2001).
[6]D. Axelrod, Traffic **2**, 764 (2001).
[7]V. Starkuviene and R. Pepperkok, Br. J. Pharmacol. **152**, 62 (2007).
[8]M. Oheim, Br. J. Pharmacol. **152**, 1 (2007).
[9]Y. Fang, A. M. Ferrie, N. H. Fontaine, J. Mauro, and J. Balakrishnan, Biophys. J. **91**, 1925 (2006).
[10]Y. Fang, A. M. Ferrie, N. H. Fontaine, and P. K. Yuen, Anal. Chem. **77**, 5720 (2005).
[11]T. P. Kenakin, Nat. Rev. Drug Discov. **8**, 617 (2009).
[12]F. Verrier, S. An, A. M. Ferrie, H. Sun, M. Kyoung, H. Deng, Y. Fang, and S. J. Benkovic, Nat. Chem. Biol. **7**, 909 (2011).
[13]Y. Fang, J. Pharmacol. Toxicol. Methods **67**, 69 (2013).
[14]A. M. Ferrie, Q. Wu, and Y. Fang, Appl. Phys. Lett. **97**, 223704 (2010).
[15]A. M. Ferrie, H. Sun, and Y. Fang, Sci. Rep. **1**, 33 (2011).
[16]K. M. Ferguson, M. B. Berger, J. M. Mendrola, H. S. Cho, D. J. Leahy, and M. A. Lemmon, Mol. Cell **11**, 507 (2003).
[17]E. Tran, H. Sun, and Y. Fang, Assay Drug Dev. Technol. **10**, 37 (2012).
[18]Y. Fang and A. Ferrie, BMC Cell Biol. **8**, 24 (2007).
[19]M. A. Pagano, J. Bain, Z. Kazimierczuk, S. Sarno, M. Ruzzene, G. Di Maira, M. Elliott, A. Orzeszko, G. Cozza, F. Meggio, and L. A. Pinna, Biochem. J. **415**, 353 (2008).
[20]H. Chew, D. S. Wang, and M. Kerker, Appl. Opt. **18**, 2679 (1979).
[21]D. C. Prieve and J. Y. Walz, Appl. Opt. **32**, 1629 (1993).